Pergamon

Chaos, Solitons & Fractals Vol. 5, Nos 3/4, pp. 461–479, 1995

0960-0779/95$9.50 + .00

0960-0779(93)E0056-H

Generic Excitable Dynamics on a Two-dimensional Map

DANTE R. CHIALVO*

Santa Fe Institute, 1660 Old Pecos Trail, Santa Fe, NM 87501, USA

Abstract—This paper introduces a two-dimensional map exhibiting several generic properties reported in excitable systems. The elementary dynamic that is analogous to that of neural elements, is analyzed using phase plane methods. Bifurcations from nonautonomous to autonomous, and from periodic to chaotic solutions are studied in a small region of parameter space. The basic implementation of distributed excitable networks using coupled maps lattices is described in one- and two-dimensional media with nearest-neighbor coupling.

1. INTRODUCTION

Excitable kinetics occurs in many biological systems including nerve, cardiac, pancreatic cells, in some chemical reactions as well as in population models [7–9, 13–15]. Bifurcations in parameter space of isolated periodically perturbed excitable systems have been extensively studied in recent years [8]. However, complex dynamics of extended excitable media, either in neural networks or in excitable media with nearest-neighbor coupling, is far less understood [15, 19]. In the numerical study of these distributed systems it is essential to simplify the description of the kinetics at one point in space (i.e. the 'local dynamics'). Thus, it is important to have a simple mathematical model with (i) generic neuronal dynamics, e.g. exhibiting most relevant properties reported in these systems; and (ii) a minimum number of parameters, optimally each one with some reasonable physical realization.

The approach presented in this paper is in the line of Kaneko [10, 11, 20] as well as Crutchfield [3] which have proposed a efficient scheme to 'coarse graining' the local dynamics at each point in space of extended dynamical systems. In this approach, which is known as coupled map lattices (CML), the dynamical system is discretized on time and space, but preserving continuous state variables. Modeling any given physical phenomena using CML is based on the following steps: (i) decompose the phenomenon into independent units (e.g. reaction, diffusion, etc); (ii) describe each unit by the simplest parallel dynamics, usually a map consisting on a transformation on each lattice point plus a coupling term among units on a given neighborhood; and (iii) solve the lattice dynamics successively, iterating in parallel the coupled maps.

The mapping function describing the local dynamics might have several forms, depending on the phenomena of interest. The logistic and circle maps, piece-wise linear maps have been extensively used to simulate specific phenomena [20]. However, maps with generic *neuron-like* dynamics has not been described.

Here a simple two-dimensional map is proposed to model the dynamics of isolated 'neurons'. We also show how this model can be introduced in a CML to represent neural networks. The paper is organized as follows. In Section 2 the minimal properties of excitable systems are reviewed and the model is defined. In Section 3, a phase plane

*e-mail address: dchialvo@santafe.edu

analysis of the dynamic is used to describe different regimes of activity found at various parameters values; the implementation of distributed coupled maps lattices is illustrated with two examples in Section 4. Section 5 discuss some additional general concerns.

2. MAPPING NEURAL EXCITABILITY

Neurons have the following global properties.

(i) In absence of external perturbation the system has an equilibrium point (usually called resting state) that is globally attracting.

(ii) The phase space is partitioned by a region (threshold) into two domains: subthreshold and suprathreshold. After a small instantaneous perturbation from the resting state which leaves the system inside the subthreshold domain, the system quickly move back to equilibrium. On the other hand, a perturbation large enough to move the system to the suprathreshold domain results in a much large excursion of the state variables before they, eventually, return to the resting state. In nerve cells, this response is called action potential.

(iii) During an action potential, and for a certain time, the system may not respond in the same manner to external perturbations. In the early phase of the action potential (known as refractory period) the threshold is moved away from the resting point, and may even transiently disappear (absolute refractory period), and then progressively relax to the asymptotic region. Therefore, the minimum amplitude of a perturbation applied during this refractory period, capable of bringing the state variables to the suprathreshold domain, is a function of time.

(iv) Under constant bias input, otherwise quiescent excitable systems may exhibit periodic oscillations. These oscillations, in some systems, and for some parameter values, may bifurcate to chaotic solutions.

We consider here these properties as belonging to 'generic neural kinetics', and any model that can account for these must involve at least two state variables. The map proposed here has the form:

$$\begin{aligned} x_{n+1} &= f(x_n, y_n) = x_n^2 \exp(y_n - x_n) + k \\ y_{n+1} &= g(y_n, x_n) = ay_n - bx_n + c \end{aligned} \tag{1}$$

where x acts as the so-called *activation* (or *potential*) variable and y as a *recovery*-like variable. Subscripts n represents iteration steps corresponding to the discretized time evolution of the system. The model includes four parameters. In the activation variable, the parameter k can act either as a constant bias or as a time-dependent additive perturbation. For $x = 0$, the fixed point y_f of the recovery variable is determined by three positive parameters: a, the time constant of recovery ($a < 1$); b, the activation-dependence of the recovery process ($b < 1$), and the offset c. Fixed points x_f, y_f of the system must simultaneously fulfill the relations:

$$\begin{aligned} x_f &= f(x_f, y_f) = x_f^2 \exp(y_f - x_f) + k \\ y_f &= g(x_f, y_f) = (c - bx_f)/(1 - a). \end{aligned} \tag{2}$$

Examination of the case $k = 0$ gives a qualitative understanding of the system. In this case, $(0, c/(1 - a))$ is always a stable point of the system since $a < 1$ (eigenvalues $= 0, a$) (see Fig. 1). Let us consider the system at rest, that is at $(0, y_{f0} = 1/(1 - a))$, assuming first that $b \ll a$ (this could be analogous to the absence of 'voltage-dependence inactivation' in real

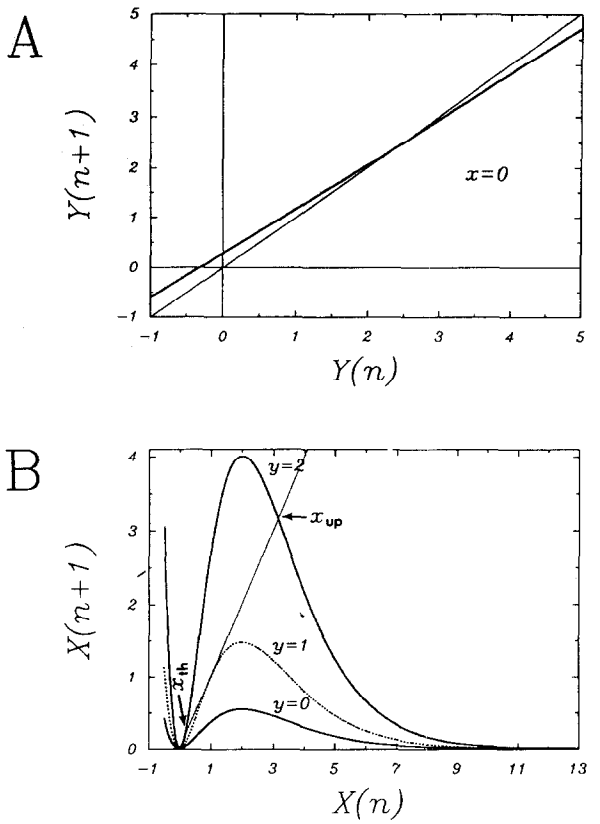

Fig. 1. Graph of equation (1) (for $a = 0.89$, $b = 0.6$, $c = 0.28$, $k = 0$). Panel A: $g(y, x)$ plotted for $x = 0$; panel B: $f(x, y)$ plotted for three values of y: 2, 1 and 0.

neurons). In this case, y is virtually frozen at y_{f0} such that the early part of the dynamics following a perturbation in x is essentially described by the iteration of the 1D map $f(x, y_{f0})$:

$$x_{n+1} = f(x_n, y_{f0}) = x_n^2 \exp(r - x_n)$$
$$r = y_{f0} = c/(1 - a). \tag{3}$$

As seen in Fig. 1(b), $x = 0$ is the unique fixed point of $f(x, y_{f0})$ when $y_{f0} < 1$, such that the system always moves back toward rest. On the other hand when $y_{f0} > 1$ $f(x, y_{f0})$ has an unstable fixed point x_{th} between 0 and 1, and a third equilibrium point x_{up} beyond $x = 1$ which might be stable or unstable. As soon as x crosses x_{th}, the dynamics changes abruptly and x starts to increase. If y was to stay constant at y_{f0}, (i.e. in the case $b \to 0$) x may converge to x_{up} (if $|df(x_{up}, y_{f0})| < 1$), return to rest with or without alternation around x_{up}, or even stays trapped in the interval $[x_{th}, f(2, y_{f0})]$. This is illustrated in Fig. 2 which shows that the bifurcation structure of $f(x, y_{f0})$ as a function of r includes a cascade of period doubling leading to chaos for initial conditions $x > 1$.

However, at $y_{f0} = 1$, $(0, y_{f0})$ is still the only fixed point of the full 2D system of equation (1), since any increase of x makes y diminish and suppress the threshold. Obviously, fixed points of the system must satisfy simultaneously both expressions in equation (2). A complete analysis is beyond the scope of this paper; we will only analyze briefly here the

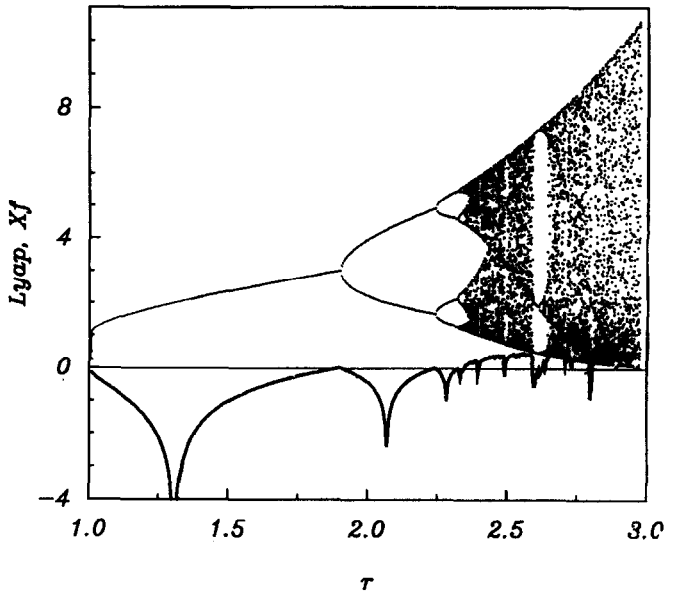

Fig. 2. Fixed point solutions (top diagram) and Lyapunov numbers (bottom diagram) of equation (3) plotted as a function of the parameter r, for initial conditions > 1 (initial conditions < 1 converge to $x = 0$). The bifurcation parameter r is the fixed point of the recovery variable in the case $b = 0$.

case $k = 0$. In that case equation (2) can be rewritten as:

$$\begin{aligned} x_f &= z(x_f) = x_f^2 \exp(y_{f0}) \exp[-(1 + \delta)x_f] \\ \delta &= b/(1 - a) > 0. \end{aligned} \tag{4}$$

A second solution with $x_f \neq 0$ appears when simultaneously:

$$\begin{aligned} 1 &= x_f \exp(y_{f0}) \exp[-(1 + \delta)x_f] \\ dz(x_f)/dx_f &= 2 - (1 + \delta)x_f = 1 \end{aligned} \tag{5}$$

which means:

$$\begin{aligned} x_f &= 1/(1 + \delta) \geqslant 1 \\ y_f &= y_{f0} - \delta/(1 + \delta) \\ &= 1 + \ln(1 + \delta) - \delta/(1 - \delta) \geqslant 1. \end{aligned} \tag{6}$$

Hence, supplementary fixed points appears from a critical value C_l such that:

$$y_{f0} = C_l/(1 - a) = 1 + \ln(1 + \delta) \geqslant 1. \tag{7}$$

For $c > C_l$, there is a pair of equilibrium points around $x = 1/(1 + \delta)$. The one below $x = 1/(1 + \delta)$ is always a saddle, the one over $x = 1/(1 + \delta)$ might be stable or unstable, but c must be chosen large enough to make it unstable. Different post-perturbation evolutions are possible depending of the number and the nature of these fixed points including the scenario similar to those described for y 'frozen' at y_{f0}. It should be noted in equation (7) that C_l, the initial value for which supplementary fixed points appears, is greater in the 2D system than for the 1D map $f(x, y_{f0})$. An example of a typical solution after a suprathreshold perturbation from the equilibrium point is illustrated in Fig. 3.

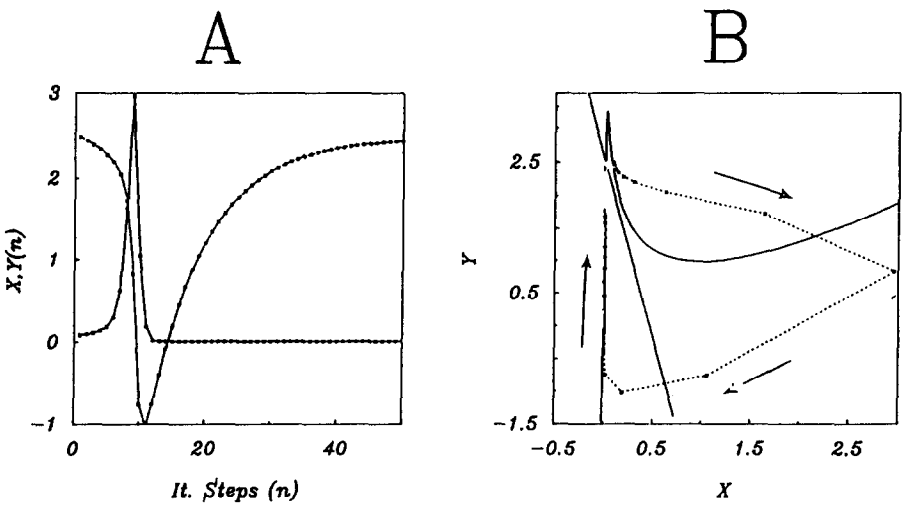

Fig. 3. Typical dynamics of equation (1) (parameters: $a = 0.89$, $b = 0.6$, $c = 0.28$, $k = 0.02$) following a supra-threshold perturbation from the resting point at time zero, both in time and on phase space. In Panel A the x-variable rises from zero first slowly then fast during the 'upstroke' of the action potential, while the y-variable decreases from its fixed point at $(c/1 - a)$ to return later, at a rate proportional to a^n. Dots are the actual values computed at each iteration step n. In panel B, the same data as in Panel A are plotted in phase space (dots connected by dotted lines). Continuous lines correspond to the nullclines of both state variables. Arrows indicate the time sequence of the cycle activation–recovery.

3. PHASE PLANE AND QUALITATIVE SOLUTIONS

Analysis of the dynamics in the phase plane is particularly useful in the study of low-dimensional nonlinear ODE systems. As in FitzHugh [6] the nullclines are plotted. These correspond to the focus of points with null derivatives for each state variable; i.e. potential and recovery. Then it becomes relatively easy to identify the equilibrium points, and to characterize the flow in its neighborhood, and it helps to describe stability and bifurcations to different attractors as parameters are changed.

A similar approach is used here to analyze equation (1). Despite the qualitative similarities between the dynamics of the map in equation (1) and that of a comparable ODE; a word of caution is necessary. Trajectories associated with iterated maps are sets of discrete points, and not continuous curves as in ODE. In two-dimensional ODE, orbits or stable and unstable manifolds partition the phase space in distinct compact subsets with their specific attractors. Structure of the stable sets might be more complicated for 2D iterated maps. As an example, one of the solutions of equation (1) is autonomous bursting and chaos (discussed later), which needs more than two dimensions in ODE models [2]. Thus, only for descriptive purposes the ODE solution's terminology is used here as analogy.

To analyze equation (1) in phase plane, we start defining the first difference of the state variables as:

$$\begin{aligned} \Delta x &= x_{n+1} - x_n \\ \Delta y &= y_{n+1} - y_n. \end{aligned} \tag{8}$$

Then the X-nullcline of equation (1) represents those y-values satisfying $\Delta x = 0$:

$$x^2 \exp^{(y-x)} + k = x \tag{9}$$

which are:

$$y = \ln(x - k) - 2\ln(x) + x, \tag{10}$$

obviously, undefined for $x \leqslant k$. The Y-nullcline of equation (1) represents all the x-values satisfying $\Delta y = 0$:

$$ay - bx + c = y \tag{11}$$

which are:

$$x = (ay + c - y)/b. \tag{12}$$

Selecting $a = 0.89$, $b = 0.6$, $c = 0.28$; (parameter values of the recovery variable used throughout this section, unless otherwise stated) the graphs of equations (10) and (12) are plotted in Panel A of Fig. 4. For the same parameter values the X-nullcline dependence over a range of k is plotted in Panel B ($k = 0.01$, 0.04, 0.08 and 0.1). The cases presented in Panel B lead to excitable (but quiescent) or to oscillatory kinetics. (for instance for $k = 0.01$ and $k = 0.04$, respectively). Notice that the nullclines' geometry [4, 9, 7, 8] is very similar to that of some two-dimensional excitable systems described in terms of ODE [13, 17, 18]. From inspection of Fig. 4 and equations (10) and (12) it is clear that, depending on parameter values, up to three nullclines' intersections are possible, as was

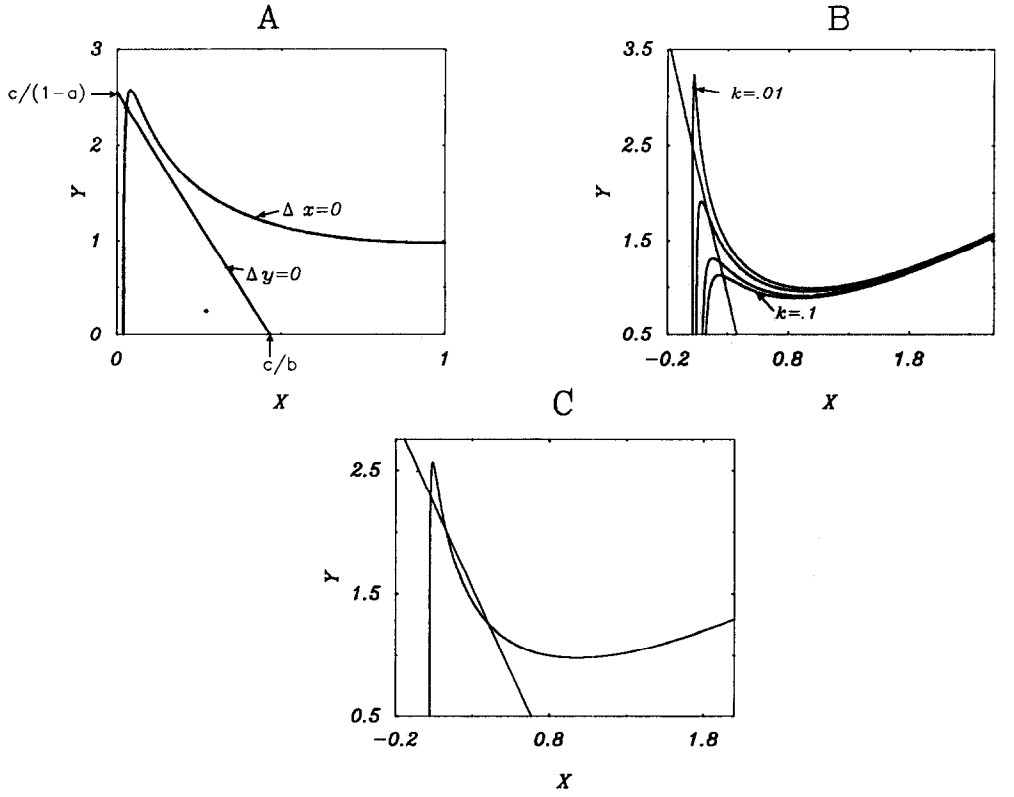

Fig. 4. Nullclines of both state variables: Panel A ($a = 0.89$, $b = 0.6$, $c = 0.28$, $k = 0.02$) shows the portion of both nullclines near the resting point. The dependence of the Y-nullcline on the recovery variable parameters a, b, c is also indicated. Panel B shows the changes of the X-nullcline as a function of the k-parameter ($k = 0.01, 0.04, 0.08, 0.1$ from top to bottom curves, recovery-variable parameters as in Panel A). Panel C shows an example of phase space containing three singular points with $a = 0.89$, $b = 0.03$, $c = 0.26$, $k = 0.02$.

demonstrated for $k = 0$ in the previous section. An example with three intersections is plotted in Panel C ($k = 0.02$, $a = 0.89$, $b = 0.3$, $c = 0.26$) where the middle one corresponds to a saddle, the one at the left is stable and the one at the right is unstable. In the following, we restrict ourselves to treat only the case of the portrait with a single singular point. The next section describes some generic dynamics found in continuous model using k as the bifurcation parameter and keeping the recovery variable parameters fixed. Increasing k in this model can be equivalent to a bias current applied to a nerve cell that progressively depolarizes its membrane potential.

3.1. *Non-autonomous solutions: excitable dynamics*

The portrait of Fig. 4 is typical of excitable dynamics. The system rests at the nullclines' intersections and may respond to a proper perturbation with an action potential. The quiescent–excitable regime will exist as long as nullclines intersect to the left of the X-nullcline maxima. The fixed point is globally attracting. From inspection of Fig. 4B, it is seen that increasing k decreases the negative slope of the X-nullcline, which (for other parameters fixed) shifts the nullclines' intersection towards conditions where the fixed point loses stability and oscillatory solutions appears. In the following paragraphs dynamics arising as k is increased are analyzed, making the correspondence with similar generic phenomenology reported in nerve cells as well as in other excitable systems. These dynamics correspond to the transition from normal to so-called supernormal recovery of excitability and from quiescent to oscillatory solutions.

3.1.1. *Normal and supernormal excitability.* In the excitable regime, action potential or subthreshold responses are initiated depending on the initial conditions (or due to a perturbation from the resting state) of the state variables. In Fig. 5, responses for representative initial conditions are presented. A section of the phase plane is depicted, where the thick solid lines are the two nullclines. Initial conditions were set at six different values near the X-nullcline. Those at the right of the nullcline (crosses joined by dotted lines: 'AP') are followed by a increase in x (i.e. an action potential similar to the one shown in Fig. 3); while those initial conditions on the left of the nullcline show a quick

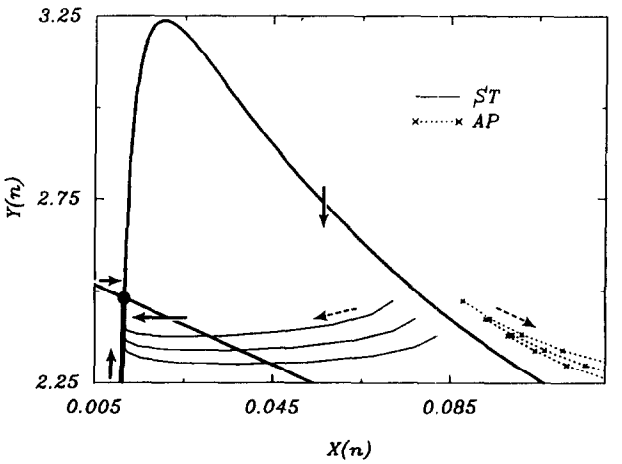

Fig. 5. Responses for six different initial conditions near the X-nullcline ($a = 0.89$, $b = 0.6$, $c = 0.28$, $k = 0.02$). Thick lines correspond to the nullclines. Lines denoted ST correspond to subthreshold evolutions and those dotted labeled AP to action potentials. Dotted arrows indicate the solutions' time sequence and continuous arrows the direction of the 'flow' direction near the nullclines.

decay (solid lines denoted 'ST') corresponding to a subthreshold response. In this context, *excitability* can be defined as the inverse as the smallest perturbation magnitude (of a single-state variable, let us say x) needed to bring the system from its actual values to those resulting in an action potential. Examining Fig. 5 and 3B, it is seen that, after an action potential, excitability returns to its maximum when the system reaches its resting point. In other words, when the system is at rest, the distance, in the x-axis, from the resting state to the separatrix between sub and suprathreshold is minimum. However, to generalize such a rule, state variables must approach the resting point monotonically; i.e. the fixed point must be a stable node. This is indeed the case in Fig. 5, because of the particular geometry of the nullclines near the point attractor. This case corresponds to what is called, in the biological literature, *normal* recovery of excitability, and the consequence is that, after an action potential is initiated, excitability grows as time passes, toward reaching the asymptotic value. Distinction has to be made with the case of *supernormal* recovery of excitability, which is characterized by a dampened oscillatory approach of the state variables to the fixed point (see below). Most nerve cells can show both modalities, depending on experimental conditions.

The transition from subthreshold responses to action potentials, for minute increases of the perturbation amplitude is, under the conditions of Fig. 5, a continuous gradation rather than an 'all-or-none' phenomenon [6]. This is generic for systems with a single intersection of the nullclines [17]. To illustrate this equation (1) was computed, in successive runs, for 30 iterations starting from several initial conditions. The recovery variable was set at its fixed point and x was incremented in each run by 10^{-7} from 0.852 to 0.853. The resulting time series are plotted, overimposed, in panel A of Fig. 6. It can be seen that very close initial conditions (at time zero) diverge with time into a continuous gradation of responses, ranging from 'full' action potentials (upward traces going off the plotted scale) to subthreshold responses. Also notice that the rising phase ('upstrokes') of the relatively low-amplitude responses (for instance the one denoted with a star) are delayed in time relative to the full responses. Such delay to activation has a finite value, here no longer than 20–30 time steps as in excitable models with N-shaped nullclines that intersect at a single resting state [17]. There are biological results showing that the latency to activation is a function of the perturbation amplitude [8], although the existence of graded responses and finite latency to activation values, generic to this phase plane scenario, is not well resolved due to experimental constraints.

The quasithreshold behavior of the model may also be visualized by plotting the maximum value reached by each response as a function of its initial condition. The resulting graph (see Fig. 6B) shows clearly that the transition from sub to suprathreshold responses is abrupt but continuous. In panel C of Fig. 6 the maximum values (same data as in panel B) and area of the responses are plotted for a relatively larger interval of initial conditions. It can be seen that both quantities, the area (dotted line) and the peak values (solid line), eventually reach a plateau for initial conditions larger than the quasithreshold. Also apparent is the oscillation of the peak amplitude, a phenomena specific to the model.

It was mentioned that trajectories, under the conditions of Figs 5 and 6, approach the resting state monotonically. However, dampened oscillatory decay to equilibrium can be found at higher k-values. An example at $k = 0.029$ is presented in Fig. 7. In panel A a section of the phase plane near the nullclines intersection is depicted. As before, initial conditions at the right of the negative-slope region of the X-nullcline results on action potentials (crosses joined by dotted lines), while initial conditions on the left decays to the resting point (solid lines). However, now the approach to the resting point follows a dampened oscillatory pattern, (i.e. the resting point is a stable focus). This oscillatory pattern is evident for both subthreshold responses and action potentials. Such pattern of

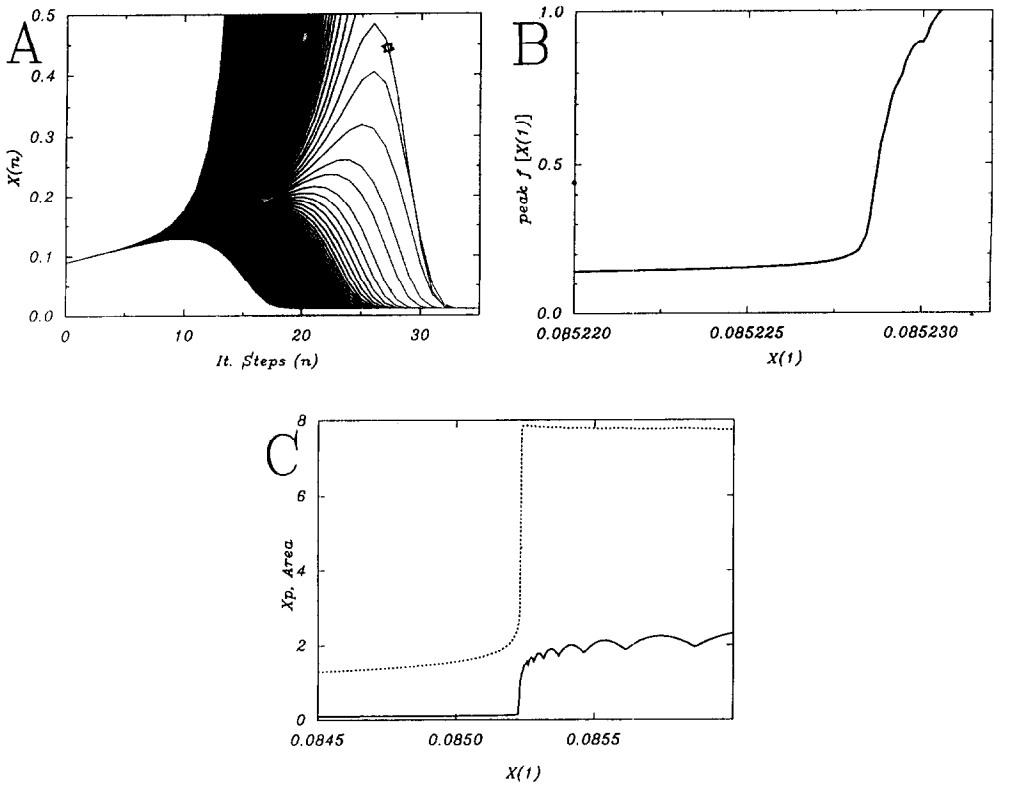

Fig. 6. Dynamics near the threshold for excitation. Panel A: initial 30 time-step solutions of equation (1) (same parameters as in Fig. 5) starting from initial conditions ($x(1)$) between 0.852 and 0.853. The recovery-variable is set at its fixed point and x is incremented in each run by 10^{-7}. Panel B: peak values of the responses in Panel A as a function of its initial condition $x(1)$. Panel C: peak value and area of sub and suprathreshold responses as a function of initial condition $x(1)$.

trajectories in phase plane will determine the particular temporal recovery of excitability called supernormal. In biological experiments this phenomena is investigated by initiating an action potential and then testing the effects of fixed amplitude perturbations applied at various delays after the action potential. A similar procedure is illustrated in Fig. 7B. The activation variable (x_n) is plotted as a function of iteration steps, overimposing six successive runs. A 'test' small perturbation is simulated by adding 0.015 to x_n in successive runs, at 20, 40, 60 and 80 time steps after the onset of the action potential. Perturbation applied at 60 time steps induces a second action potential while stimuli applied earlier or later results in subthreshold responses. Notice that the occurrence of the action potential coincide with the small oscillation overshoot in the x-variable. In contrast, under normal recovery of excitability, a second action potential can be elicited only up to a given minimum delay while shorter test intervals results always in subthreshold responses.

3.2. *Autonomous solutions: oscillatory dynamics*

Further increases in k-value results in a bifurcation from the quiescent–excitable to oscillatory solutions. For $k \simeq 0.03$ the nullclines intersect near the negative slope region of the X-nullcline resulting in the coexistence of a stable focus and a stable oscillatory solution. Convergence to either attractor depends on initial conditions. This is illustrated in Fig. 8, which shows the section of the phase plane containing the fixed point. Trajectories

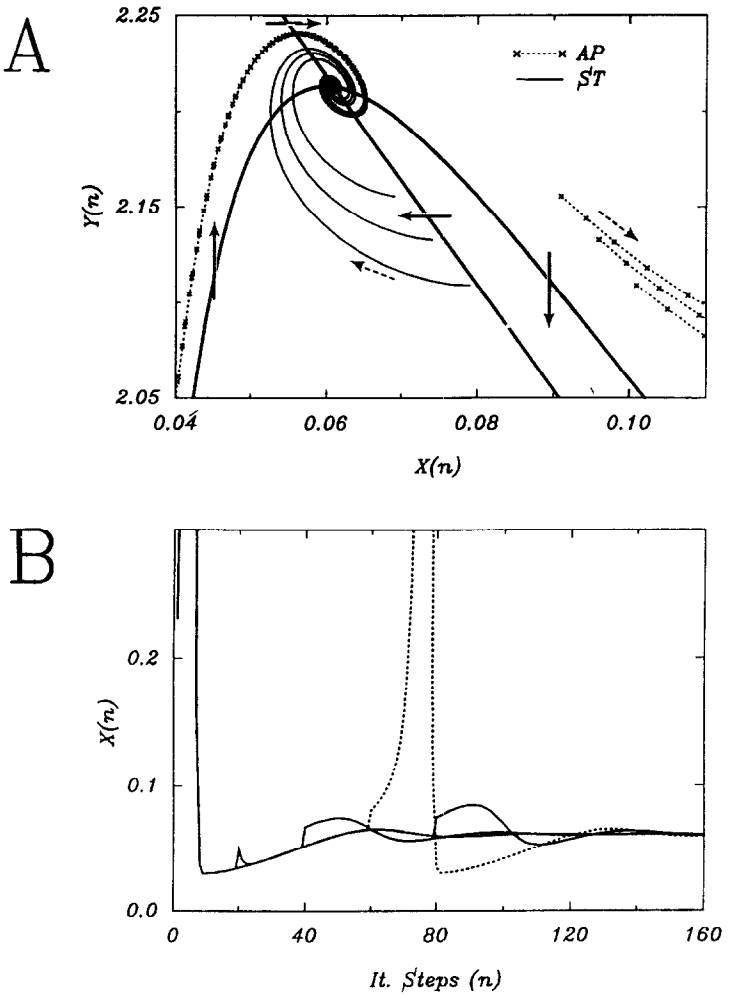

Fig. 7. Supernormal recovery of excitability for $k = 0.029$ (other parameters as in Fig. 5). Panel A shows the section of the phase plane containing the resting point. As in Fig. 6 initial conditions at the right of the X-nullcline dome results in action potentials (crosses joined by dotted lines), while initial conditions on the left decays to the resting point (solid lines). Notice the oscillatory approach to the equilibrium point. Panel B shows the activation variable (x_n) plotted as a function of iteration steps, superimposing six successive runs. The effect of small perturbation to x_n is tested at 20, 40, 60 and 80 time-steps after the onset of an action potential. Perturbation applied at 60 time-steps induces a second action potential (dotted trace) while same stimuli applied earlier or latter results in subthreshold responses.

initiated outside the 'limit cycle' converge to it (crosses joined by dotted line, denoted 'LC'), while initial conditions close to the fixed point spiral into the resting state (solid line denoted 'FP'). Here we do not discuss the details or the nature of the separatrix defining basins of attraction for these two solutions. The coexistence of these attractors implies that it is possible to switch between these two solutions by applying a single perturbation of proper timing and magnitude. To illustrate this, equation (1) was computed from initial conditions resulting in a 'limit cycle' (see Fig. 8, panels B and C). Then, at a particular time-step a small perturbation affecting the activation variable was added (at $n = 225$ it was set $x_n = x_n + 0.07$). The perturbation shifted the state variables (arrow from A to B in Fig. 8B and C) inside the domain of attraction of the fixed point, which was followed by a spiraling to the resting point. This phenomena, also called 'annihilation' of pacemaker

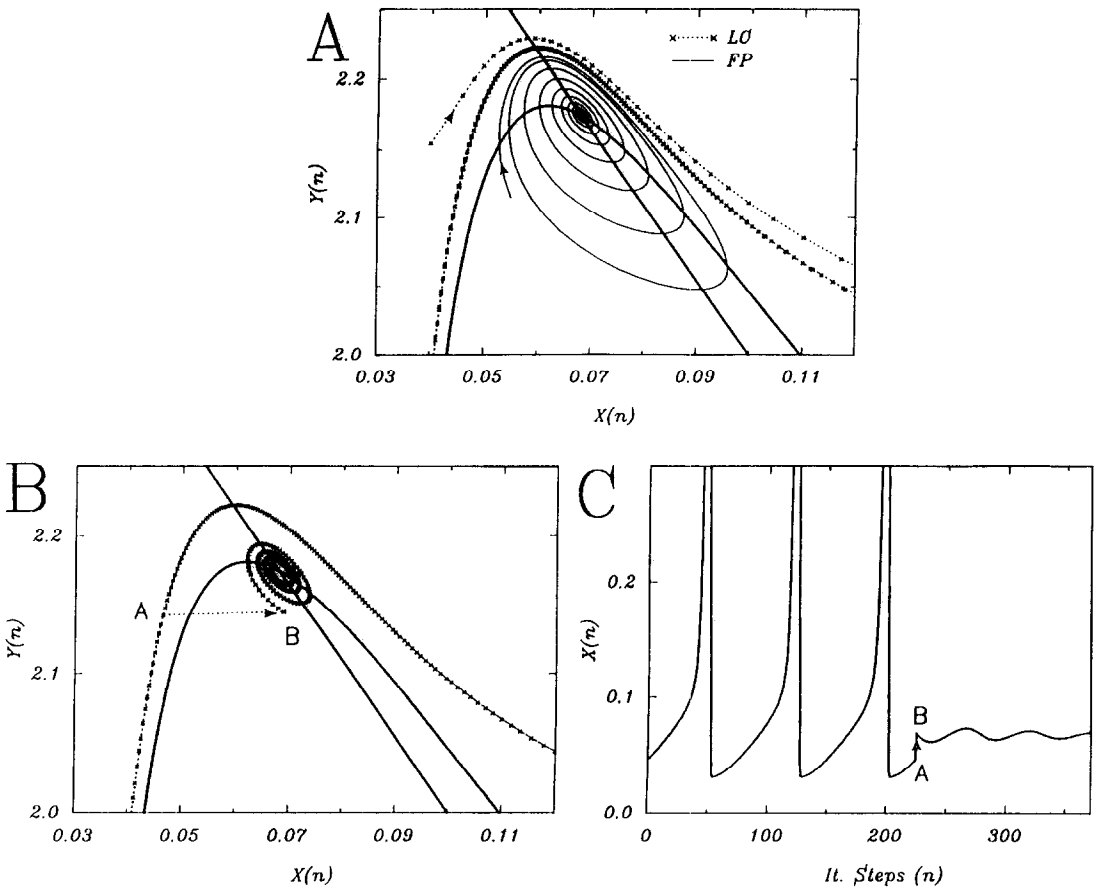

Fig. 8. Bistability of oscillatory and quiescent solutions for $k = 0.03$ (other parameters as in Fig. 5). Panel A: trajectories initiated outside the 'limit cycle' converge to it (crosses joined by dotted line, denoted 'LC'), initial conditions close to the fixed point converge to its (solid line denoted 'FP'). Panels B and C show the switching, in phase space and time domains, respectively, from oscillations to equilibrium resulting from a single perturbation (applied at point 'A') that moves the state variables (to point 'B') inside the domain of attraction of the fixed point.

activity, has been reproduced in various experimental settings, including squid giant axons, cardiac Purkinje fibers, and sinus node cells and numerically in model of nerve and cardiac cells [1, 6, 14, 15].

As k is increased further, the amplitude of the oscillations diminishes, until it finally vanishes when a stable fixed point reappears at the nullclines' intersection. Figure 9 shows the variation of the relative frequency and the amplitude of the oscillation as a function of increasing k. The relative frequency was estimated as the number (normalized to 2 in this figure) of action potentials counted on a fixed number of iterations, and amplitude refers to the averaged maximum value of x during each oscillation. Starting at $k \simeq 0.03$ there are oscillatory solutions in a wide range of k-values. As k increases, their frequency increases monotonically, whereas the amplitude of the oscillations decreases after an initial increase. There is remarkable similarity between these results and comparable computations done in the space-clamped Hodgkin–Huxley equations (see, for example, ref. [16] for comparison).

3.2.1. *Bursting and chaos.* Solutions described so far can be qualitatively understood considering the properties of the (apparently generic) phase plane. However, for specific

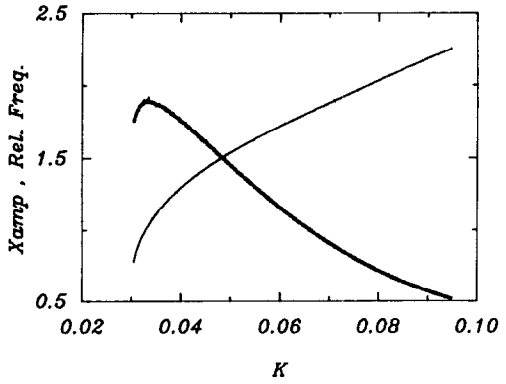

Fig. 9. Peak amplitude (thick line) and relative frequency of oscillations (thinner line) as a function of k.

parameter values, we have observed complicated autonomous solutions. These dynamics include autonomous bursting and aperiodic solutions, resembling much dynamics observed experimentally and numerically [2] in continuous systems with more than two degrees-of-freedom. The necessary conditions for aperiodic oscillations to occur are the following: (i) there must be a single unstable fixed point, such that the system has autonomous oscillations; (ii) the activation–dependence of the recovery variable (parameter b in equation (1)) must be relatively small, such that $f(x, y)$ in (1) is not substantially modified by the ongoing oscillations (in other words y stays more or less 'frozen' at y_{f0} as discussed in Section 2, see also Fig. 1B); (iii) the unstable fixed point must be near x, $y = 1$, 1 (the reason will become apparent below). For instance, shifting b from 0.6 to 0.18 moves the system from the oscillations described in the previous section (obtained at parameters: $a = 0.89$, $b = 0.6$, $c = 0.28$ and $k = 0.03$) to aperiodic bursting solutions.

An example of the x- and y-time series and the respective phase plane plot corresponding to this dynamics is shown in Fig. 10. The basic rhythm is composed by sets of initially relatively large oscillations, which may be followed by one or more rapid secondary oscillations of increasing amplitude. The interval between large spikes as well as the number of small oscillations are both variable. Note also that 'trajectories' drawn in the

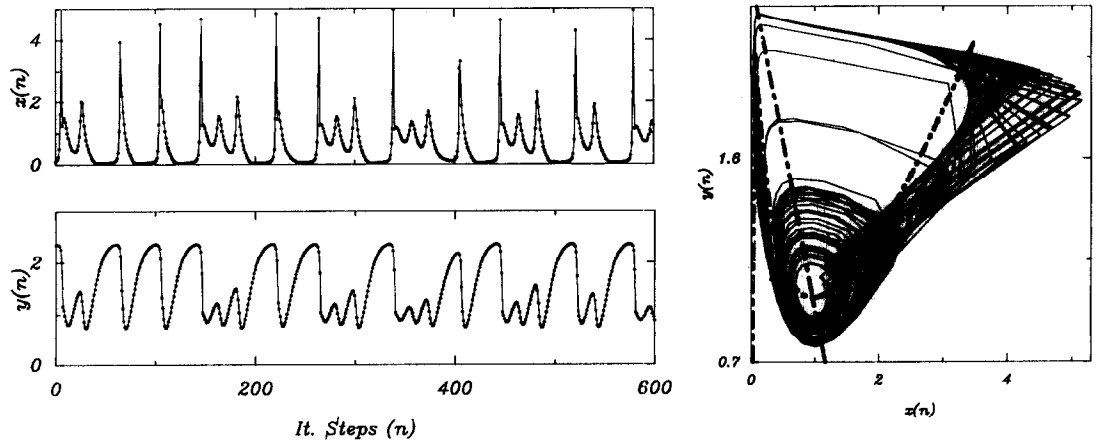

Fig. 10. Chaotic solutions ($a = 0.89$, $b = 0.18$, $c = 0.28$, $k = 0.03$). Time series correspond to the state variables (top: $x(n)$, bottom: $y(n)$) and the diagram on the right side to the phase space plot of the same values on the traces. Thick dotted lines in the phase space plot correspond to the nullclines.

phase plane plot of Fig. 10 intersect in the two-dimensional space during bursts. Bursting-like solutions appear, since the value of the activation-dependence of the recovery variable, b, allows several iterates of the map around the unstable fixed point (near $x, y = 1, 1$) before spiraling out to produce a large oscillation. In the interval ($b = 0.15$ to 0.3) where complex oscillations occur, there are multiple regions at which the largest Lyapunov exponent is positive, indicating chaotic dynamics, mixed with several windows of periodic dynamics. Work is still needed to fully understand the bifurcation structure of equation (1) in the range of these complicated solutions.

4. DISTRIBUTED SYSTEMS: ILLUSTRATIVE EXAMPLES

For the discussion of the implementation of distributed excitable media using coupled map lattices it might be useful to think, besides neural elements, also of models of forest-fire propagation assuming a very large time and space scale. In that, x in equation (1) can be thought of as representing the 'local temperature' of a given tree, and y as its 'local height'. An isolated tree of a given height will burn to ashes, providing that the local temperature is elevated up to a certain threshold. Eventually, after the temperature decreases, trees will re-grow to an (idealized) asymptotic height (i.e. y_{f0} in (1)). A fire initiated at a given point of a full-grown forest will increase the temperature (let assume by simple diffusion) of the surrounding trees. Fire propagation will ensue, providing that the distance between trees and the heat transference are adequate. Let us combine the former two conditions on a coupling constant $0 > d < 1$. Then a single row of trees can be simulated by formulating the diffusion of the local temperature x in (1) as:

$$x^i_{n+1} = (1 - d)f(x^i_n) + (d/2)[f(x^{i+1}_n) + f(x^{i-1}_n)] \tag{13}$$

where subscripts n represent the time-step, and superscripts i a lattice point ($i = 1, 2, \ldots, I$ = system size) with certain boundary conditions. The 'diffusion' constant d can be fixed or distributed with some probability through a given neighborhood, depending on the specific problem being modeled. It is usual to iterate only once the coupling scheme of equation (13) following each iteration of the local dynamics. However, if the problem at hand requires a finer resolution, diffusion can be conveniently rescaled by iterating more than once the coupling scheme before proceeding with the next iteration of the local dynamics.

In two-dimensions a forest with four nearest-neighbor coupling is written as:

$$x^{i,j}_{n+1} = (1 - d)f(x^{i,j}_n) + (d/4)[f(x^{i+1,j}_n) + f(x^{i-1,j}_n) + f(x^{i,j+1}_n) + f(x^{i,j-1}_n)] \tag{14}$$

where superscripts i, j define a point of the square lattice of size I, J.

In the examples presented in the next paragraphs the dynamics of equation (1) with the appropriate coupling term might be pictured as waves on a biological excitable tissue or as combustion waves in a forest fire model. The present model is used in the following to illustrate two simple phenomena relatively well understood in excitable media. These are the phenomena of 'vulnerability' to reentry on a ring, and the existence of stable periodic solutions in 2D media. This section is only a numerical exercise to show the model behavior in simulating simple dynamics on extended media. There are no new results in what follows, since the phenomenology illustrated is already understood.

4.1. *Vulnerability, unidirectional block and re-entry on a ring*

Unidirectional block of propagation, leading to permanent circulation of waves in a one-dimensional ring of excitable elements, is a classic problem. The experimental

observation in biological excitable tissues goes back to Mines [12]. The rate-dependency of wave propagation velocity is crucial to understand that phenomenon. Fifty excitable maps were coupled as in equation (13), with $d = 0.4$ and periodic boundary conditions. Figure 11 represents, in perspective, the space, i, on the horizontal axis ('cell' 1 at left, 'cell' 50 at right), time, n, running from present, at the front, to the future on the back of the figure, and x_n^i the activation variable of each i-cell at time n on the vertical axis.

Each cell has parameter values, such that in absence of perturbation they are quiescent at the resting point ($a = 0.89$, $b = 0.6$, $c = 0.28$, $k = 0.02$). Cell 1 is stimulated in all the panels once at time-step zero. That initial stimulus induces two propagated waves circulating in opposite directions, which eventually collide and die in the middle of the ring in all cases. After that initial stimulation a second perturbation (always amplitude = 0.3, at cell 35 through 37) is tested at four different times. In Panel A, the extra perturbation is added at time-step 50, originating another pair of waves which eventually will collide. In panel B, the second perturbation is applied at time-step 42, which also creates two waves, but now one of them propagates slower than the other. The reason for that delay is the fact that, initially, the wave circulating from right to left 'runs' into cells which are less recovered from the first propagated wave. Conversely the wave front propagating from left to right runs into more and more recovered units. (Roughly, speed of propagation is a function of coupling and of amplitude of the x-variable, which in turn is a function of the recovery variable, see below). In panel C, stimulation at time-step 41 yields a unidirectional block, leading to self-sustained re-excitation of the ring. Finally, if the extra

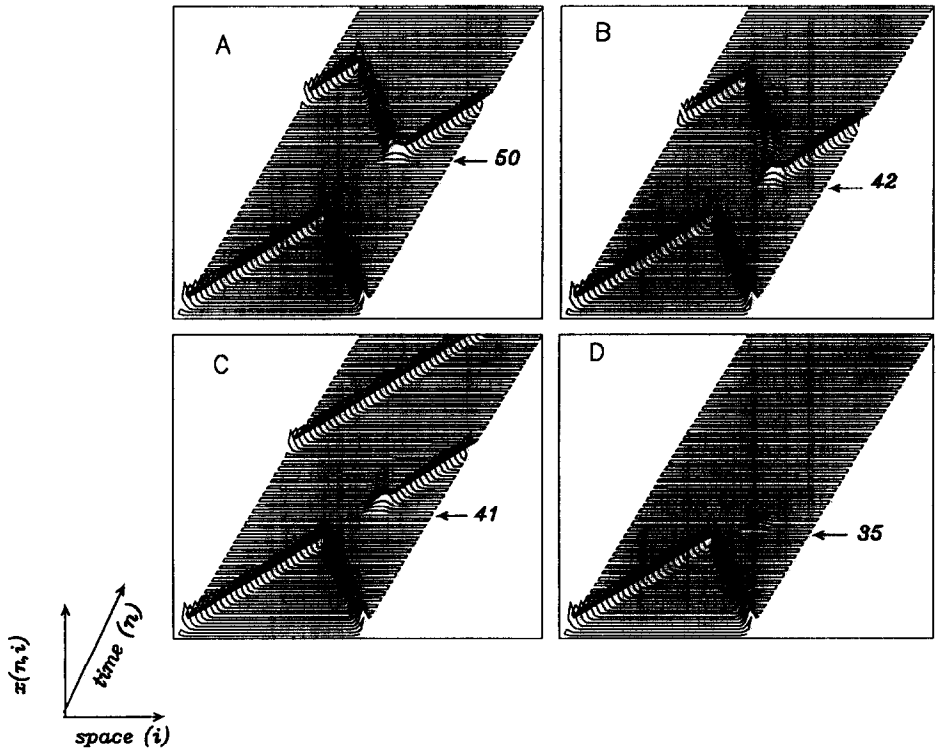

Fig. 11. Unidirectional block and re-entry on a ring. An initial wave front is initiated in each panel stimulating cell 1. A second perturbation is applied to cells 35 to 37 at time-step 50 in panel A, 42 in B, 41 in C, and at 35 in Panel D. Stimuli at a critical timing (between 41 and 36 in this example) result in unidirectional propagation and self re-excitation of the ring.

perturbation is applied sooner ($t = 35$, Panel D) the excitation is not propagated, since the stimulus comes at a time when the recovery variable is still far from equilibium.

In generic excitable media, wave propagation depends on the period of excitation. If the re-excitation occurs very late, propagation velocity will be faster than if it occurs earlier, as was shown in the previous example. Figure 12 shows the computed velocity as a function of the period of excitation. Calculations were done as follows. A ring of 100 elements was connected as in Fig. 11, and a circulating wave was initiated with appropriate initial conditions. After transients decayed, the speed of circulation was calculated, detecting 100 passages of the wave through a given element and expressed as the average space units propagated on an iteration step. The number of elements was progressively shortened by one unit and similar computations were repeated. Two curves are plotted in Fig. 12, one obtained for $k = 0.02$ the other for $k = 0.029$. Notice that the former shows a monotonic decrease of speed as the period shortened, where the latter exhibits an initial overshoot. The behavior of the speed vs period in these two cases is exactly what must happen, considering that the parameter values correspond to local dynamics of either 'normal' ($k = 0.02$) or 'supernormal' ($k = 0.029$) recovery of excitability as it was shown in previous sections.

4.2. *Self-organized solutions in two-dimensional media*

Spiral waves of various forms are periodic solutions known to exist in two-dimensional excitable media [14, 15]. An isolated vortex can be initiated with proper spatial initial conditions, and will rotate autonomously in an otherwise quiescent excitable two-dimensional media. In the case of a two-variable excitable model like equation (1) it is sufficient to start the simulation with a specific gradient of the activation-variable orthogonal to another gradient in the recovery variable. This is illustrated in Fig. 13. A 100×100 lattice is simulated according to equations (1) and (14). Parameter values ($a = 0.89$, $b = 0.6$, $c = 0.26$, $k = 0.02$) correspond to excitable quiescent local dynamics. The activation variable at time zero is set as $x^{i,j} = i \times 0.0033$ and the recovery variable as $y^{i,j} = y_f - (j \times 0.0066)$. The first four panels of Fig. 13 illustrate the initial evolution of such initial conditions for iteration steps 0 to 4 in two different ways. Diagrams on the right show the nullclines as well as the entire lattice x- vs y-values mapped on phase space. Panels on the left side show the values of x at each lattice point and, in addition, the

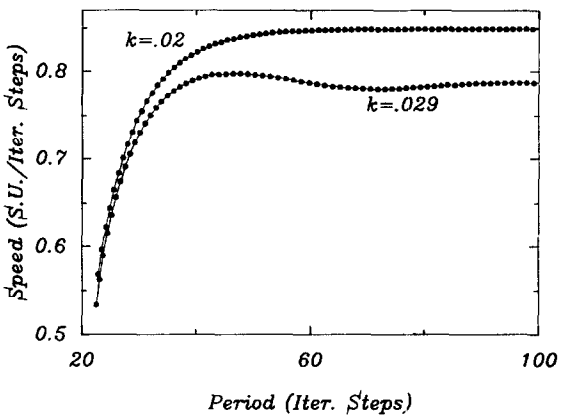

Fig. 12. Propagation velocity as a function of re-excitation period computed on a ring of initial length equal to 100 elements. Length is progressively decreased, and the average number of units (S.U.) traveled on a iteration step is plotted for the two modalities of excitability recovery: normal ($k = 0.02$) and supernormal ($k = 0.029$).

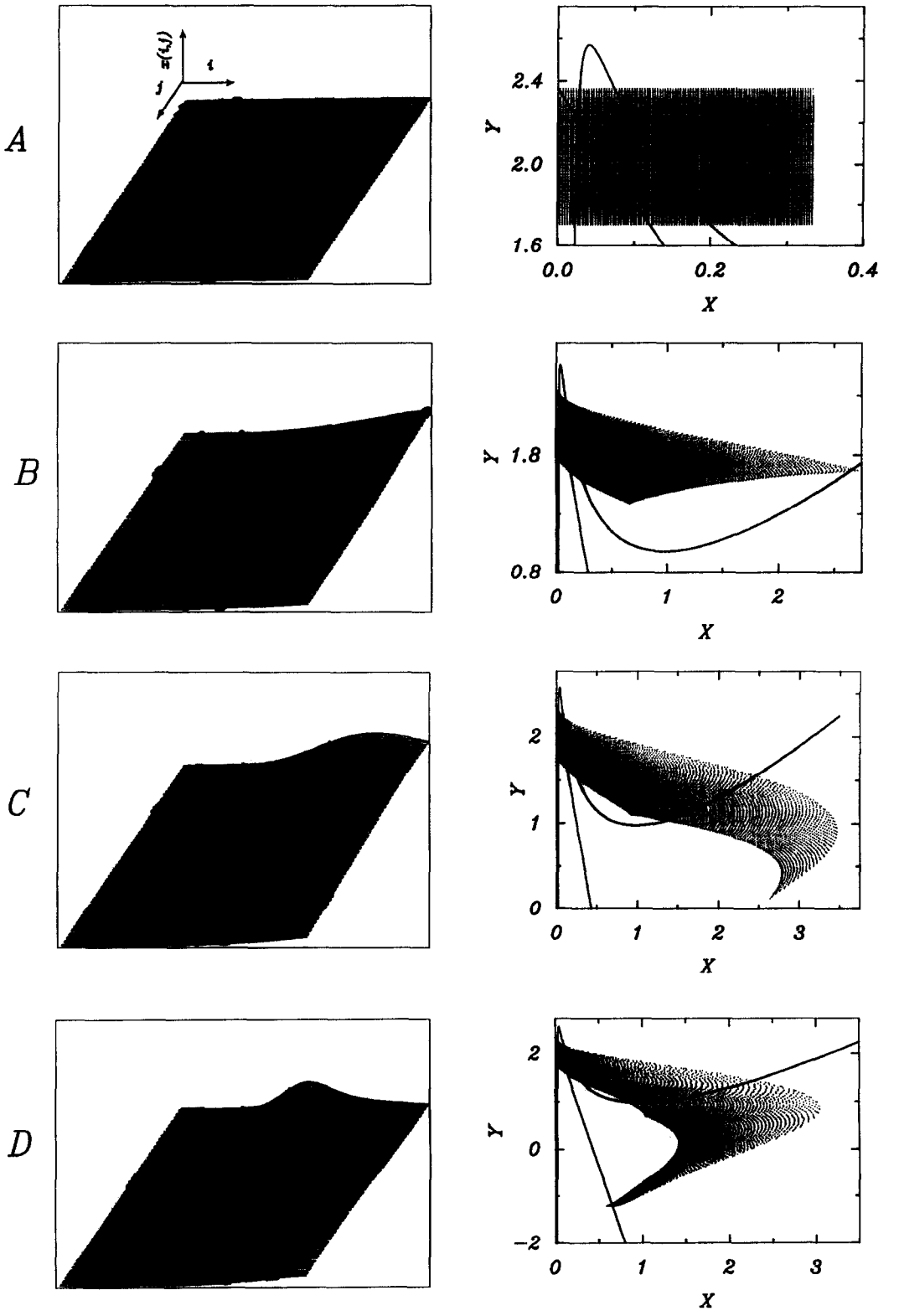
A
x(i,j)
i
j
Y
2.4
2.0
1.6
0.0
0.2
0.4
X
B
Y
1.8
0.8
0
1
2
X
C
Y
2
1
0
0
1
2
3
X
D
Y
2
0
−2
0
1
2
3
X

Fig. 13. (A)–(D).

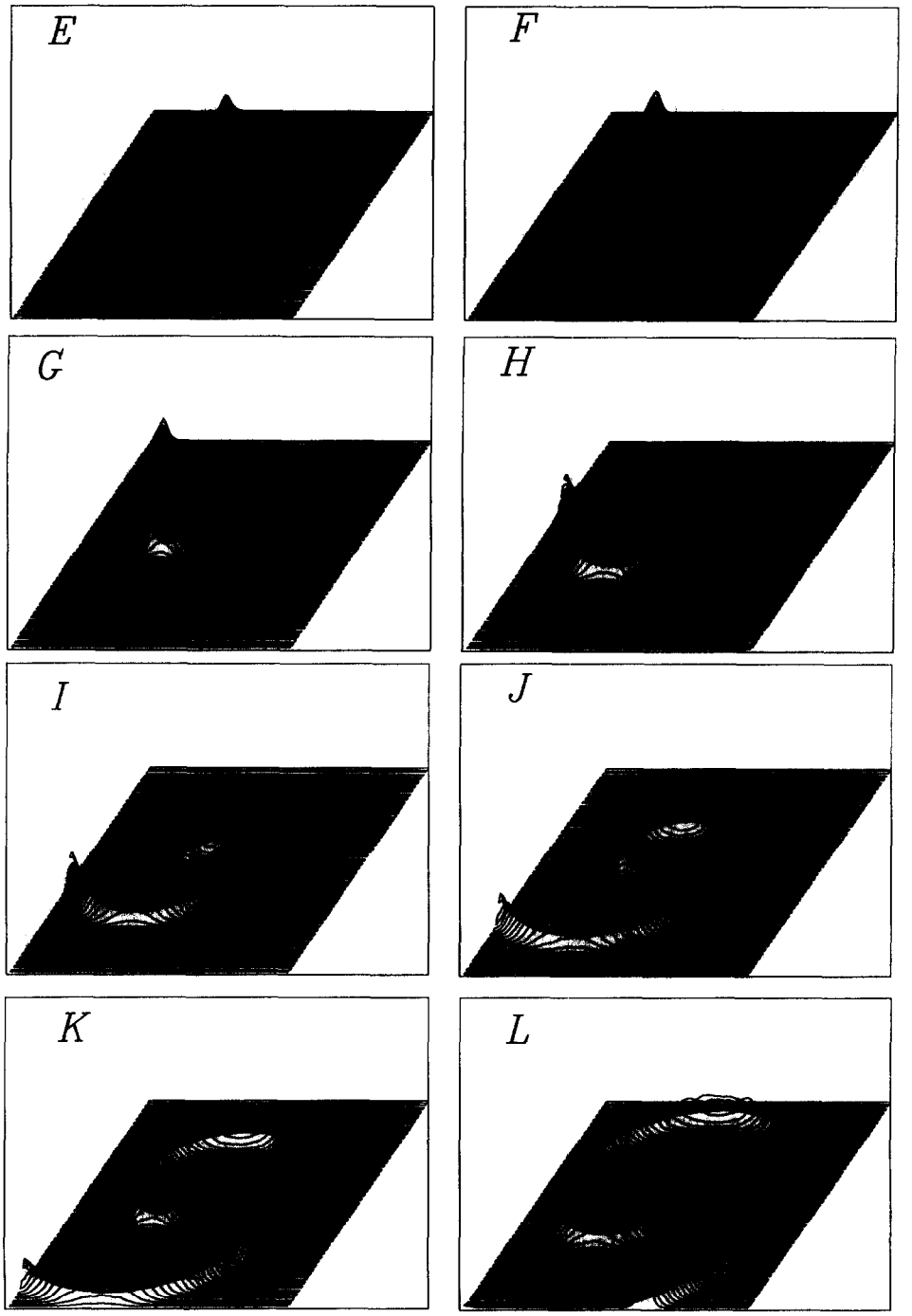

Fig. 13. Single spiral wave in simulated 2D excitable media. Panels A to D: plots correspond to time steps 0, 2, 3, 4 after setting the initial conditions as explained in the text showing the formation of a propagating wave. Diagrams on the right are the phase planes, where the entire 100×100 lattice x-, y-pairs (dots) are plotted as well as the nullclines (continuous lines). Diagrams on the left correspond to the three-dimensional projection of the lattice $x(i, j)$ states. Also are marked (darkened) those i, j points in the lattice with state variable values near the X- or Y-nullclines. Panels E to L are the three-dimensional projections of the lattice $x(i, j)$ states for time-steps 10, 20, 30, 40, 50, 60, 70 and 80, respectively, showing the formation of a broken wave (panel E, F) that reached a critical curvature (panel G–H) to eventually leading to a spiral wave (panels I–L).

nullclines are mapped on the space by identifying those cells with state variables near the nullcline (± 0.001) (denoted in black in the figure). From simple inspection of both plots in Panel A it can be seen that the initial conditions span a 'family' of possible evolutions. There are units which are at or very near the resting point (those at the intersection of both nullclines), units that will undergo an action potential (those at the top right of the phase space corresponding also at the top right of the spatial plot) and units that will go relatively quickly to the resting point (those at the left of both plots). Also notice that this initial conditions implies that cells at the bottom of both plots are 'less recovered' than cells at the top. With that in mind, it is then trivial to predict which cells will give rise to a propagated solution (if any): the x-variable of the top right corner grows first (see Panel B) followed by those units at the bottom right (see Panel C). Then, a traveling wave begins to propagate from right to left, and the respective phase plane plot starts filling a full activation-recovery cycle, as is seen already in Panel D. However, the bottom half of the wave front propagates slower that the top half, since it is running on (and into) less recovered media. Eventually, after 20 time-steps, the wave front will be reduced to the top half (see Panels E and F). At 30 time-steps the tip of the wave starts to curve, propagating to regions of its own wake that have now recovered; as well as propagating to the bottom right corner. Once that the tip has reached a critical curvature, (see Panels G–H) the density of 'current' seen by a unit situated in between the tip and the wake of such curved wave front will be the highest at any place on the media. As soon as such cells recover they will be re-excited to some degree, to become the 'tip' of the spiral wave around which the entire vortex keep rotating. (see panels G to L corresponding to time-steps 30 through 80 respectively). The theory, here only just sketched for illustrative purposes, is far more complicated and is extensively discussed in refs [14, 15].

5. CONCLUSIONS

This paper shows that a very simple two-dimensional map with few parameters suffices to reproduce many simple, as well as some more complicated, dynamics reported in neurons and in other excitable systems. Besides the phenomenology illustrated in this paper, we have also verified that equation (1) can account for other specific dynamics demonstrated in perturbed excitable systems. This includes the phase-resetting of an ongoing oscillation by a single stimuli (which Fig. 8 is only a particular case) and the organization in parameter space of phase-locked responses to periodic pulsatile perturbations. Overall, these results indicate that the model is generic of a large class of systems.

The thrust of the approach discussed in this paper is on its 'macroscopic' view of neuronal dynamics, as opposed to the fine resolution of ODE or PDE models. In addition, maps like equation (1) can collapse higher dimensions on a few relevant (as in the case of bursting discussed previously) while preserving the richness and complexity of the dynamics but reducing numerical (and computational) demands.

Obviously, the simplicity of this approach may not be the best choice if we attempt to replicate quantitatively specific details of a given excitable system. For instance, if neurons are the object of interest, we might choose from several well-elaborated models derived from the original formulation of Hodgkin and Huxley that will reproduce each specific detail of isolated *in vitro* neuronal dynamics. Then, if a supercomputer is available, very large arrays of interconnected compartmental neuron models can be simulated. Providing that the role of dozens of parameters embedded in each of the thousands of equations manageable, some results will eventually come out. In that regard we favor a quoted warning about the risk of such effort specially when those are 'too successful' [11]:

> Conventionally, a model equation in physics is believed to have a one-to-one correspondence with a phenomenon in concern. For example, if one tries to model turbulence one often adopts molecular dynamics or a PDE which has a fair basis on the phenomena at the level of microscopic process. If one succeeds in reproducing the phenomena from the model equation, then what can one learn? What one might obtain is just that the equations are correct or reasonable, without any understanding of the complex phenomena.

In the other end of the modeling arsenal we find the all-discrete 'macroscopic' cellular automata (CA), which, indeed with very few simple rules can accommodate for several generic phenomena seen in excitable systems. However, some relevant dynamics require large number of (more sophisticated) rules. In that case an important drawback to consider is very well expressed in a recent review [5]:

> In creating more rules, some of the advantages of CA are defeated: speed and conceptual simplicity. Since these more complex models elude analysis and take considerably longer to simulate, one should be cautious in trying to push CA behind their inherent strengths.

If the interest is to understand complex dynamics arising in large distributed neural media and to overcome the difficulties pointed out by the above quotes, then the model discussed in this paper will probably be of some use.

Acknowledgments—I would like to thank Alain Vinet and Andre Longtin for many useful discussions related and unrelated with this work. Early conversations with K. Kaneko are also greatly appreciated. This work was partially supported by the National Institute of Mental Health, under grant R01-MH50064-02.

REFERENCES

1. E. N. Best, Null space in the Hodgkin–Huxley equations: a critical test, *Biophys. J.* **27**, 87–104 (1979).
2. T. R. Chay, Chaos in a three variable model of an excitable cell, *Physica* **D16**, 233–242 (1985).
3. J. P. Crutchfield and K. Kaneko, Phenomenology of spatiotemporal chaos, In *Directions in Chaos*. World Scientific, Singapore (1987).
4. L. Edelstein-Keshet, *Mathematical Models in Biology*. Random House, New York (1988).
5. G. B. Ermentrout and L. Edelstein-Keshet, Cellular automata approaches to biological modeling, *J. Theor. Biol.* **160**, 97–133 (1992).
6. R. FitzHugh, Impulses and physiological states in theoretical models of nerve membrane, *Biophys. J.* **1**, 445–466 (1961).
7. A. Golbeter, *Rythmes et chaos dans lest systemes bichimiques et cellulaires*. Masson, Paris (1990).
8. L. Glass and M. Mackey, *From Clocks to Chaos. The Rhythms of Life*. Princeton University Press, Princeton, NJ (1988).
9. A. E. Jackson, *Perspectives of Nonlinear Dynamics*, Vols 1, 2. Cambridge University Press, Cambridge (1990).
10. K. Kaneko, Simulating physics with coupled map lattices, in *Formation, Dynamics and Statistics of Patterns*, edited by K. Kawasaki. World Scientific, Singapore, (1989).
11. K. Kaneko, Coupled map lattice, in *Chaos Order and Patterns*, edited by Artuso *et al*. Plenum, New York (1991).
12. G. R. Mines, On circulating excitations in heart muscle and their possible relation tachycardia and fibrillation, *Trans. R. Soc. Can.* **4**, 43–52 (1914).
13. J. D. Murray, *Mathematical Biology, Biomathematics* **19**, edited by S. A. Levin. Springer, Berlin (1990).
14. A. T. Winfree, *The Geometry of Biological Time, Biomathematics* **8**, edited by K. Krickeberg and S. A. Levin. Springer, Berlin (1980).
15. A. T. Winfree, *When Time Breaks Down: The Three-dimensional Dynamics of Electrochemical Waves and Cardiac Arrhythmias*. Princeton University Press, Princeton NJ (1987).
16. J. Rinzel, On repetitive activity in nerve, *Fed. Proc.* **37**, 2793–2802 (1978).
17. J. Rinzel and G. B. Ermentrout, Analysis of neural excitability and oscillations, in *Methods in Neuronal Modeling: From Synapses to Networks*, edited by C. Koch and I. Segev, pp. 135–171. MIT Press, Cambridge, MA (1988).
18. L. A. Segel, *Modeling Dynamic Phenomena in Molecular and Cellular Biology*. Cambridge University Press, Cambridge (1984).
19. H. L. Swinney and V. I. Krinsky, *Waves and Patterns in Chemical and Biological Media*, reprinted from *Physica* **D49** (1991). MIT Press, Cambridge, MA and Elsevier, Amsterdam (1992).
20. K.Kaneko, editor, Theory and applications of coupled map lattices, in *Nonlinear Science: Theory and Applications*, edited by A. V. Holden. Wiley, Chichester (1993).